Dynamic phase transition of the Blume-Capel model in an oscillating magnetic field

Erol Vatansever[1] and Nikolaos G. Fytas[2]
[1]*Department of Physics, Dokuz Eylül University, TR-35160 Izmir, Turkey*
[2]*Applied Mathematics Research Centre, Coventry University, Coventry CV1 5FB, United Kingdom*

(Received 24 November 2017; revised manuscript received 23 December 2017; published 17 January 2018)

We employ numerical simulations and finite-size scaling techniques to investigate the properties of the dynamic phase transition that is encountered in the Blume-Capel model subjected to a periodically oscillating magnetic field. We mainly focus on the study of the two-dimensional system for various values of the crystal-field coupling in the second-order transition regime. Our results indicate that the present nonequilibrium phase transition belongs to the universality class of the equilibrium Ising model and allow us to construct a dynamic phase diagram, in analogy with the equilibrium case, at least for the range of parameters considered. Finally, we present some complementary results for the three-dimensional model, where again the obtained estimates for the critical exponents fall into the universality class of the corresponding three-dimensional equilibrium Ising ferromagnet.

DOI: 10.1103/PhysRevE.97.012122

I. INTRODUCTION

Although our understanding of equilibrium critical phenomena has developed to the point where well-established theories and results are available for a wide variety of systems, far less is known for the physical mechanisms underlying the nonequilibrium phase transitions of many-body interacting systems. In this respect, theoretical but also experimental studies deserve particular attention in order to provide further insight into the universality and scaling principles of this type of phenomenon. We know today that when a ferromagnetic system, below its Curie temperature, is exposed to a time-dependent oscillating magnetic field, it may exhibit a fascinating dynamic magnetic behavior, which cannot be directly obtained via its corresponding equilibrium part [1]. In a typical ferromagnetic system being subjected to an oscillating magnetic field, there occurs a competition between the time scales of the applied field period and the metastable lifetime, τ, of the system. When the period of the external field is selected to be smaller than τ, the time-dependent magnetization tends to oscillate around a nonzero value, which corresponds to the dynamically ordered phase. In this region, the time-dependent magnetization is not capable of following the external field instantaneously. However, for larger values of the period of the external field, the system is given enough time to indeed follow the external field. Hence, in this case the time-dependent magnetization oscillates around its 0 value, indicating a dynamically disordered phase. When the period of the external field becomes comparable to τ, a dynamic phase transition takes place between the dynamically ordered and the disordered phases.

Up to now, there have been several theoretical [2–21] and experimental [22–26] studies regarding dynamic phase transitions, as well as the hysteresis properties of different types of magnetic materials. These works indicate that, in addition to the temperature, both the amplitude and the period of the time-dependent magnetic field play a key role in dynamical critical phenomena. On the other hand, and to the best of our knowledge, there exist only a few studies focusing on the critical exponents and universality aspects of spin models driven by a time-dependent oscillating magnetic field [27–33]. In particular, by means of Monte Carlo simulations and finite-size scaling analysis, it has been suggested that the critical exponents of the two-dimensional (2D) kinetic Ising model are compatible to those of the corresponding 2D equilibrium Ising model [27–29]. In another relevant work [30], Buendía and Rikvold used soft Glauber dynamics to estimate the critical exponents of the same system, providing strong evidence that the characteristics of the phase transition are universal with respect to the choice of the stochastic dynamics. The above results have been corroborated by a numerical study of the triangular-lattice Ising model [33], where the obtained critical exponents were found to be consistent within errors to those of the equilibrium Ising counterpart. Furthermore, the universality features of the 3D kinetic Ising model have been clarified by Park and Pleimling [31]: the critical exponents of the 3D kinetic Ising model are in good agreement with those of the corresponding equilibrium 3D case. Last but not least, the role of surfaces in nonequilibrium phase transitions has been elucidated in Ref. [34], where the nonequilibrium surface exponents were found not to coincide with those of the equilibrium critical surface, and even more recently the fluctuations in a square-lattice ferromagnetic model driven by a slowly oscillating field with a constant bias have been studied in Ref. [35]. The latter work provided us with the ubiquitous reminder that the equivalence of the dynamic phase transition to an equilibrium phase transition is limited to the critical region near the critical period and zero bias.

It is evident from the above discussion that most of the numerical work performed to clarify the universality classes of dynamic phase transitions has been devoted to the kinetic spin-1/2 Ising type of models. Still, there is another suitable candidate model in which the above predictions may be tested: the so-called Blume-Capel model [36,37]. The Blume-Capel model is defined by a spin-1 Ising Hamiltonian with a single-ion uniaxial crystal-field anisotropy (or simpler crystal-field

coupling) Δ [36,37] [see also Eq. (1) below]. The fact that this model has been very widely studied in statistical and condensed-matter physics is explained not only by its relative simplicity and the fundamental theoretical interest arising from the richness of its phase diagram, but also by a number of different physical realizations of variants of the model [38,39]. From the theoretical point of view, in order to have a better understanding of the equilibrium phase transition characteristics, the model and its variants have been intensively studied by making use of different methods, such as renormalization-group calculations [40–42], Monte Carlo simulations [43–51], and mean-field-theory approaches [52–54].

Despite intensive investigations devoted to the determination of time-dependent magnetic-field effects on the dynamic phase transition nature of the spin-1 Blume-Capel model [8,15,16,18,55,56], critical exponents and universality properties of the model have not been elucidated. To fill this gap, we present in this paper the first study of universality of the spin-1 square-lattice Blume-Capel model in the neighborhood of a dynamic phase transition under the presence of a time-dependent magnetic field. The aim of our study is twofold: First, we would like to check how the critical exponents of the kinetic spin-1 Blume-Capel model, estimated at various values of Δ in the second-order transition regime, compare to those of the corresponding equilibrium Ising model. Second, we target the construction of a dynamic phase diagram on the related plane for the range of Δ values considered. In a nutshell, our results indicate that the dynamic phase transition of the present kinetic system belongs to the universality class of the equilibrium Ising model. Some complementary results obtained for the 3D version of this spin-1 kinetic model, presented at the end of this paper, provide additional support in favor of this claim. Furthermore, the obtained dynamic phase diagram is found to be qualitatively similar to the equilibrium phase diagram constructed on the crystal-field–temperature plane [45,47,51]. Last but not least, the data given in this study qualitatively support previously published studies, where general dynamic phase transition features of the same system have been investigated via mean-field-theory [15,16] and effective-field-theory [18] treatments.

The outline of the remaining parts of the paper is as follows: In Sec. II we introduce the model and the details of our simulation protocol. In Sec. III we define the relevant observables that will facilitate our finite-size scaling analysis for the characterization of the universality principles of this dynamic phase transition. The numerical results and discussion of the 2D and 3D models are presented in Secs. IV and V, respectively. Finally, Sec. VI presents a summary of our conclusions.

II. MODEL AND SIMULATION DETAILS

We consider the square-lattice Blume-Capel model under the existence of a time-dependent oscillating magnetic field. The Hamiltonian of the system reads as

$$\mathcal{H} = -J \sum_{\langle xy \rangle} \sigma_x \sigma_y + \Delta \sum_x \sigma_x^2 - h(t) \sum_x \sigma_x, \qquad (1)$$

where the spin variable σ_x takes on the value $-1, 0$, or $+1$, $\langle xy \rangle$ indicates summation over nearest neighbors, and $J > 0$ is the ferromagnetic exchange interaction. Δ denotes the crystal-field coupling and controls the density of vacancies ($\sigma_x = 0$). For $\Delta \to -\infty$ vacancies are suppressed and the model becomes equivalent to the Ising model. The term $h(t)$ corresponds to a spatially uniform periodically oscillating magnetic field, and, following the prescription in Refs. [29–31], we assume that all lattice sites are exposed to a square-wave magnetic field with amplitude h_0 and half-period $t_{1/2}$.

The phase diagram of the equilibrium Blume-Capel model on the crystal-field–temperature plane consists of a boundary that separates the ferromagnetic from the paramagnetic phase. The ferromagnetic phase is characterized by an ordered alignment of ± 1 spins. The paramagnetic phase, on the other hand, can be either a completely disordered arrangement at high temperatures or a ± 1-spin gas in a spin-0-dominated environment at low temperatures and high crystal fields. At high temperatures and low crystal fields, the ferromagnetic-paramagnetic transition is a continuous phase transition in the Ising universality class, whereas at low temperatures and high crystal fields the transition is of first-order character [36,37]. The model is thus a classic and paradigmatic example of a system with a tricritical point $[\Delta_t, T_t]$ [38], where the two segments of the phase boundary meet. A most recent reproduction of the phase diagram of the model can be found in Ref. [51], and an accurate estimation of the location of the tricritical point has been given in Ref. [50]: $[\Delta_t, T_t] = [1.9660(1), 0.6080(1)]$. However, for the needs of the current work we restricted our analysis to the second-order transition regime of the model $\Delta < \Delta_t$. In particular, we studied the system at the following crystal-field values: $\Delta = 0, 0.5, 1, 1.5$, and 1.75.

In numerical grounds, we performed Monte Carlo simulations on square lattices with periodic boundary conditions using the single-site update Metropolis algorithm [57–59]. This approach, together with the alternative option of stochastic Glauber dynamics [60], comprises the standard recipe in kinetic Monte Carlo simulations, as also noted in Ref. [30]. In fact, very recently, the surface phase diagram of the 3D kinetic Ising model in an oscillating magnetic field has been studied within the framework of both Glauber and Metropolis dynamics and it has been shown that the results remain qualitatively unchanged when different single-spin flip dynamics are used [32].

In our simulations, $N = L \times L$ defines the total number of spins and L the linear dimension of the lattice, taking values within the range $L = 32-256$. For each pair of (L, Δ) parameters we performed several independent long runs, tailored to the value of Δ under study, using the following protocol: the first 10^3 periods of the external field have been discarded during the thermalization process and numerical data were collected and analyzed during the following 10^4 periods of the field. We note that the time unit in our simulations is one Monte Carlo step per site (MCSS) and that error bars have been estimated using the jackknife method [59]. To set the temperature scale we fixed units by choosing $J = 1$ and $k_B = 1$, where k_B is the Boltzmann constant. Appropriate choices of the magnetic-field strength, $h_0 = 0.2$, and the temperature, $T(\Delta) = 0.8 T_c(\Delta)$, ensured that the system is in the multidroplet regime [31]. Here, $T_c(\Delta)$ denotes the set of critical temperatures of the equilibrium square-lattice Blume-Capel model, as estimated in Ref. [47]

TABLE I. Summary of estimates for the critical half-period $t^c_{1/2}$, the critical exponent ν, and the magnetic exponent ratio γ/ν of the spin-1 kinetic Blume-Capel model for various values of the crystal-field coupling Δ, as listed. The second column lists the critical temperatures of the equilibrium Blume-Capel model, as estimated in Ref. [47].

Δ	T_c [47]	$t^c_{1/2}$	ν	γ/ν
0.00	1.693(3)	206.4 ± 1.2	1.05(8)	1.74(3)
0.50	1.564(3)	166.6 ± 1.1	1.01(7)	1.75(1)
1.00	1.398(2)	112.3 ± 1.3	1.03(9)	1.75(2)
1.50	1.151(1)	61.0 ± 0.3	0.98(6)	1.76(1)
1.75	0.958(1)	43.1 ± 0.2	1.02(6)	1.76(2)

and also reported in Table I. Finally, for the application of finite-size scaling to the numerical data, we have restricted ourselves to data with $L \geqslant L_{\min}$. As usual, to determine an acceptable $L_{\min}$ we employed the standard χ^2 test of goodness of fit [61]. Specifically, the p value of our χ^2 test is the probability of finding an χ^2 value which is even larger than the one actually found from our data. We considered a fit to be fair only if $10\% < p < 90\%$.

A similar prescription was also followed for the study of the 3D version of the model and the details of this implementation are given at the beginning of Sec. V.

III. OBSERVABLES

In order to determine the universality aspects of the kinetic Blume-Capel model, we consider the half-period dependencies of various thermodynamic observables. The main quantity of interest is the period-averaged magnetization

$$Q = \frac{1}{2t_{1/2}} \oint M(t)dt, \tag{2}$$

where the integration is performed over one cycle of the oscillating field. Given that for finite systems in the dynamically ordered phase the probability density of Q becomes bimodal, one has to measure the average norm of Q in order to capture symmetry breaking, so that $\langle |Q| \rangle$ defines the dynamic order parameter of the system. In Eq. (2), $M(t)$ is the time-dependent magnetization per site,

$$M(t) = \frac{1}{N} \sum_{x=1}^{N} \sigma_x(t). \tag{3}$$

To characterize and quantify the transition using finite-size scaling arguments we must also define quantities analogous to the susceptibility in equilibrium systems. The scaled variance of the dynamic order parameter

$$\chi_L^Q = N\left[\langle Q^2 \rangle_L - \langle |Q| \rangle_L^2\right] \tag{4}$$

has been suggested as a proxy for the nonequilibrium susceptibility, also theoretically justified via fluctuation-dissipation relations [17]. Similarly, one may also measure the scaled variance of the period-averaged energy

$$\chi_L^E = N\left[\langle E^2 \rangle_L - \langle E \rangle_L^2\right], \tag{5}$$

so that χ_L^E can be considered the relevant heat capacity of the dynamic system. Here E denotes the cycle-averaged energy corresponding to the cooperative part of the Hamiltonian, (1):

$$E = \frac{1}{2t_{1/2}N} \oint \left[-J \sum_{\langle xy \rangle} \sigma_x \sigma_y + \Delta \sum_x \sigma_x^2 \right] dt. \tag{6}$$

A few comments are in order at this point with respect to the use of Eqs. (5) and (6), where we focus only on the cooperative part of the energy in order to calculate the time-averaged energy over a full cycle of the external field and its corresponding variance. Conceptually, the role of the time-averaged energy originating from an oscillating magnetic field (namely, the time-dependent Zeeman term) can be better understood with the help of the dynamic correlation function. In spin systems driven by a time-dependent external field there may be some dynamic correlations between the time-dependent magnetic field and the time-dependent magnetization, which strongly depend on the chosen temperature, including other parameters as well. In order to explain this point in detail, let us define the dynamic correlation function $G = \langle M(t)h(t) \rangle - \langle M(t) \rangle \langle h(t) \rangle$, where $\langle \dots \rangle$ denotes the time average over a full cycle of the external field [4]. Since $\langle h(t) \rangle = 0$, we are allowed to simplify as $G = \langle M(t)h(t) \rangle$. We know that in the relatively strong ferromagnetic phase the spin-spin interactions are dominant against the field energy. Therefore, the spins do not tend to respond to the varying magnetic field for fixed system parameters. In other words, the corresponding dynamic correlation function is almost 0 in this region. In the regions, except from the strongly ferromagnetic and paramagnetic phases, the relevant term may have a nonzero value, however, the energy term coming from this type of behavior does not affect the true dynamic phase transition point [6].

Finally, with the help of the dynamic order parameter Q we may define the corresponding fourth-order Binder cumulant [27,28]

$$U_L = 1 - \frac{\langle |Q|^4 \rangle_L}{3\langle |Q|^2 \rangle_L^2}, \tag{7}$$

which provides us with an alternative estimation of the critical point, at the same giving time a flavor of universality at its intersection point [62].

IV. RESULTS AND DISCUSSION

It may be useful at this point to briefly describe the mechanism underlying the dynamical ordering that takes place in kinetic ferromagnets, as exemplified in Figs. 1 and 2 for the case of the $\Delta = 1$ Blume-Capel model and a system size of $L = 128$. In particular, Fig. 1 presents the time evolution of the magnetization and Fig. 2 the period dependencies of the dynamic order parameter Q. Several comments are in order at this point: For slowly varying fields [Fig. 1(a)] the magnetization follows the field, switching every half-period. In this region, as expected, $Q \approx 0$, as also shown by the blue line in Fig. 2. On the other hand, for rapidly varying fields [Fig. 1(c)] the magnetization does not have enough time to switch during a single half-period and remains nearly constant for many successive field cycles, as also illustrated by the black line in Fig. 2. In other words, whereas in

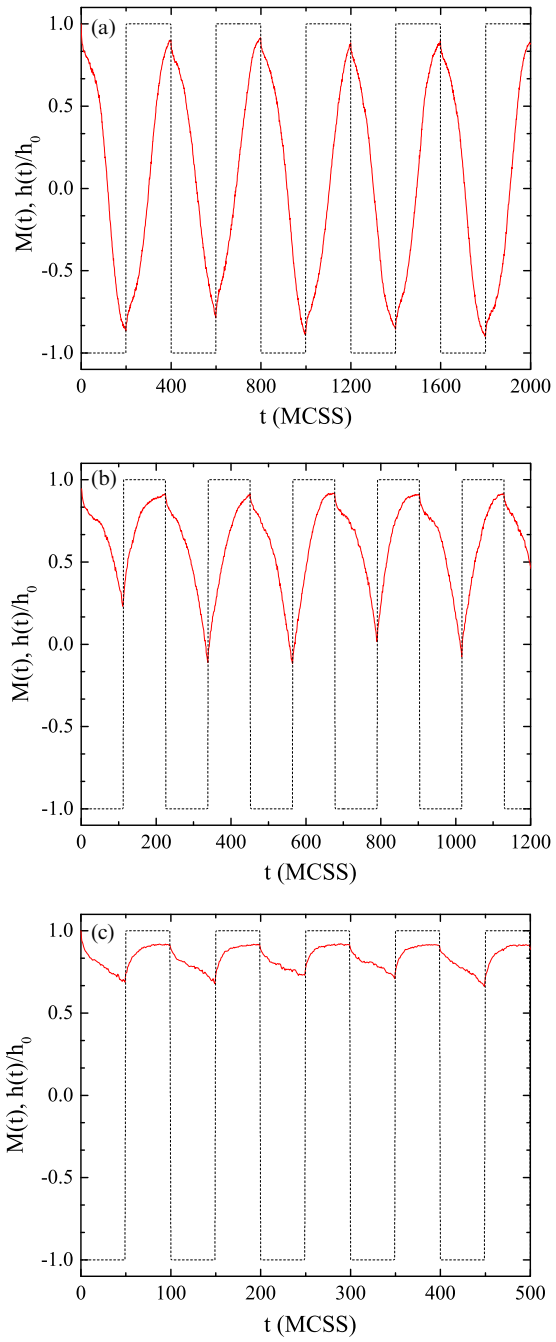

FIG. 1. Time series of the magnetization (solid red curves) of the $\Delta = 1$ kinetic spin-1 Blume-Capel model under the presence of a square-wave magnetic field (dashed black lines) for $L = 128$ and three values of the half-period of the external field: (a) $t_{1/2} = 200$ MCSS, corresponding to a dynamically disordered phase; (b) $t_{1/2} = 113$ MCSS, close to the dynamic phase transition; and (c) $t_{1/2} = 50$ MCSS, corresponding to a dynamically ordered phase. Note that for the sake of clarity the ratio $h(t)/h_0$ is displayed.

the dynamically disordered phase the ferromagnet is able to reverse its magnetization before the field changes again, in the dynamically ordered phase this is not possible and therefore the time-dependent magnetization oscillates around a finite value. The competition between the magnetic field and the metastable state is captured by the half-period parameter $t_{1/2}$

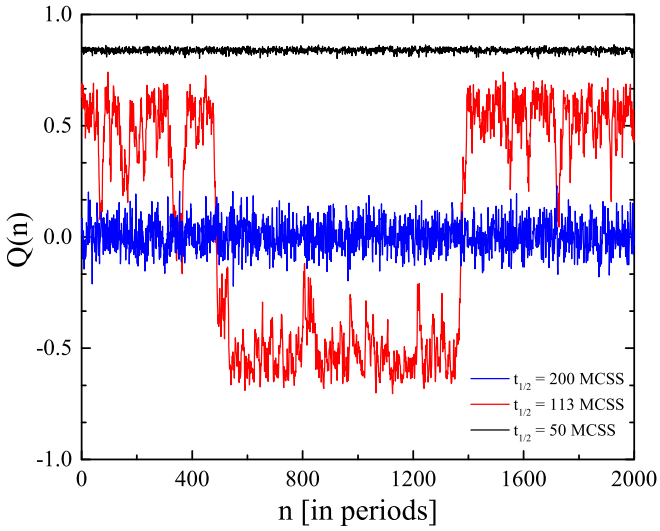

FIG. 2. Period dependencies of the dynamic order parameter of the $\Delta = 1$ kinetic spin-1 Blume-Capel model for $L = 128$. Results are shown for three characteristic cases of the half-period of the external field: $t_{1/2} = 200$ MCSS (blue line), $t_{1/2} = 113$ MCSS (red line), and $t_{1/2} = 50$ MCSS (black line). The strongly fluctuating trace (red line) corresponds to the vicinity of the dynamic phase transition, given that $t_{1/2} \approx t_{1/2}^{c} = 112.3 \pm 1.3$, as shown below.

(or by the normalized parameter $\Theta = t_{1/2}/\tau$, with τ being the metastable lifetime [31]). Obviously, $t_{1/2}$ plays the role of the temperature in the corresponding equilibrium system. Now, the transition between the two regimes is characterized by strong fluctuations in Q [see Fig. 1(b) and the evolution of the red line in Fig. 2]. This behavior is indicative of a dynamic phase transition and occurs for values of the half-period close to the critical one $t_{1/2}^{c}$ (otherwise stated, when $t_{1/2} \approx \tau$, so that $\Theta \approx 1$). Of course, since the value $t_{1/2} = 113$ MCSS used for this illustration is slightly higher than the value of $t_{1/2}^{c}$ for the case $\Delta = 1$ (see Table I), the observed behavior also includes some nonvanishing finite-size effects.

To illustrate the spatial aspects of the transition scenario described in Figs. 1 and 2, we also show the configurations of the local order parameter $\{Q_x\}$ in Fig. 3 for the case of the $\Delta = 1.75$ Blume-Capel model and a system of linear size $L = 128$. When the period of the external field is selected to be larger than the relaxation time of the system, above $t_{1/2}^{c}$ [see Fig. 3(a)], the system follows the field in every half-period, with some phase lag, and $Q_x \approx 0$ at all sites x. In other words the system lies in the dynamically disordered phase. On the other hand, below $t_{1/2}^{c}$ [see Fig. 3(c)], the majority of spins spend most of their time in the $+1$ state, i.e., in the metastable phase during the first half-period and in the stable equilibrium phase during the second half-period, except for equilibrium fluctuations. Thus most $Q_x \approx +1$. The system is now in the dynamically ordered phase. Near $t_{1/2}^{c}$ and the expected dynamic phase transition, there are large clusters of both $+1$ and -1 states, within a sea of 0-state spins, as clearly illustrated in Fig. 3(b).

However, the value of the local order parameter $\{Q_x\}$ does not distinguish between random distributions of $\sigma_x = \pm 1$ and regions of $\sigma_x = 0$. To highlight this distinction, we present in

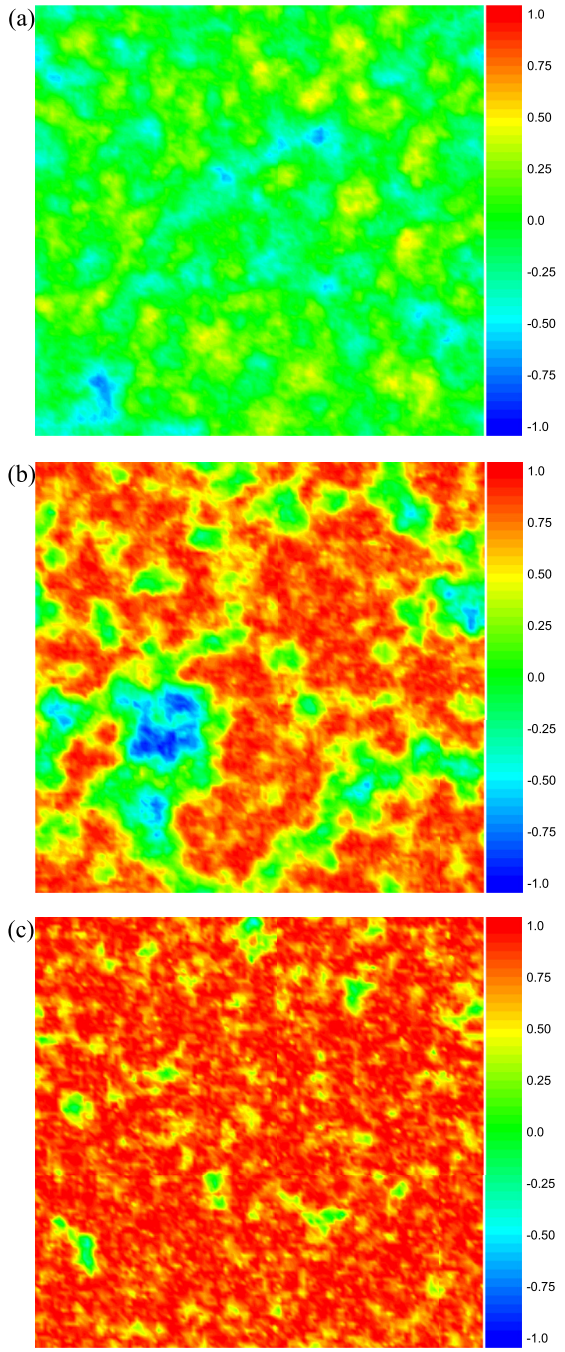

FIG. 3. Configurations of the local dynamic order parameter $\{Q_x\}$ of the $\Delta = 1.75$ kinetic spin-1 Blume-Capel model for $L = 128$. The "snapshots" of $\{Q_x\}$ for each regime are the set of local period-averaged spins during some representative period: (a) $t_{1/2} = 100$ MCSS $> t_{1/2}^c$, dynamically disordered phase; (b) $t_{1/2} = 43$ MCSS $\approx t_{1/2}^c$, near the dynamic phase transition; and (c) $t_{1/2} = 20$ MCSS $< t_{1/2}^c$, dynamically ordered phase.

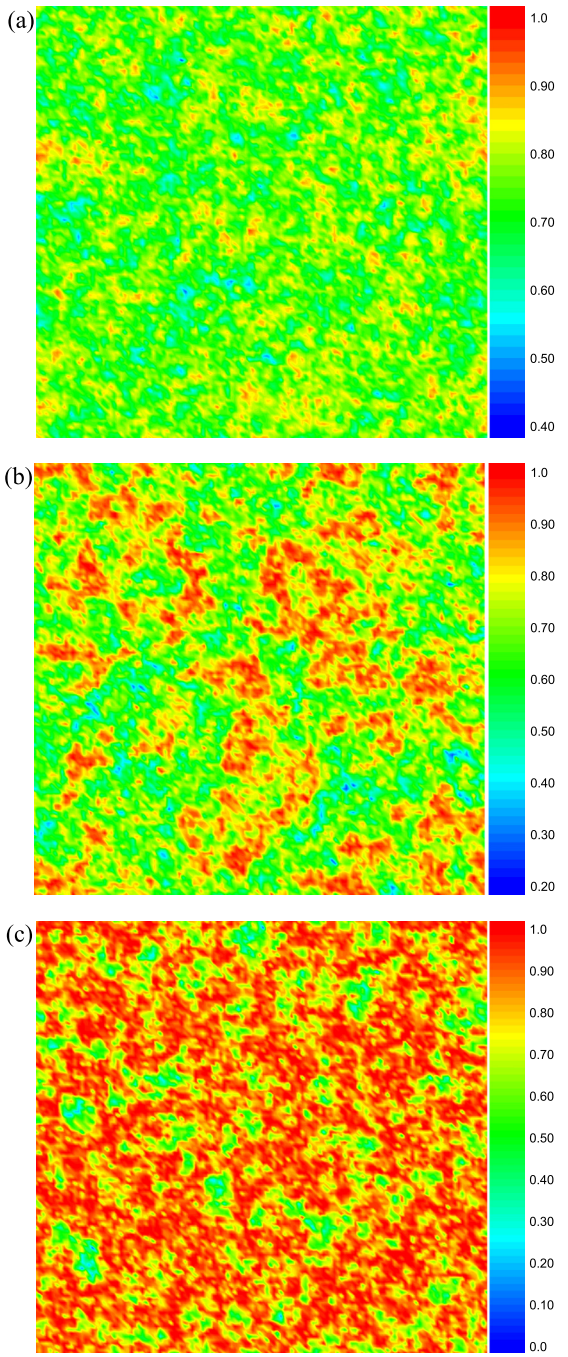

FIG. 4. In full analogy with Fig. 3 we show snapshots of the period-averaged quadrupole moment conjugate to the crystal-field coupling Δ. Simulation parameters are exactly the same as those used in Figs. 3(a)–3(c).

Fig. 4 similar snapshots of the dynamic quadrupole moment over a full cycle of the external field, $O = \frac{1}{2t_{1/2}} \oint q(t)dt$, where $q(t) = \frac{1}{N} \sum_{x=1}^{N} \sigma_x^2$. The simulation parameters are exactly the same as those used in Figs. 3(a)–3(c). Of course, the dynamic quadrupole moment is always 1 for the kinetic spin-1/2 Ising model, because $\sigma_x = \pm 1$ in this case. In the spin-1 Blume-Capel model the density of the ($\sigma_x = 0$) vacancies is controlled by the the crystal-field coupling Δ, and, thus the value of the dynamic quadrupole moment changes depending on Δ. When the value of Δ increases, starting from its Ising limit ($\Delta \to -\infty$), the number of vacancies also increases in the system, so that the dynamic quadrupole moment tends to decrease from its maximum value. In Fig. 4, except for the red regions, indicating the $+1$ state, regions enclosed by finite values exemplify the role played by the the crystal-field coupling in the system.

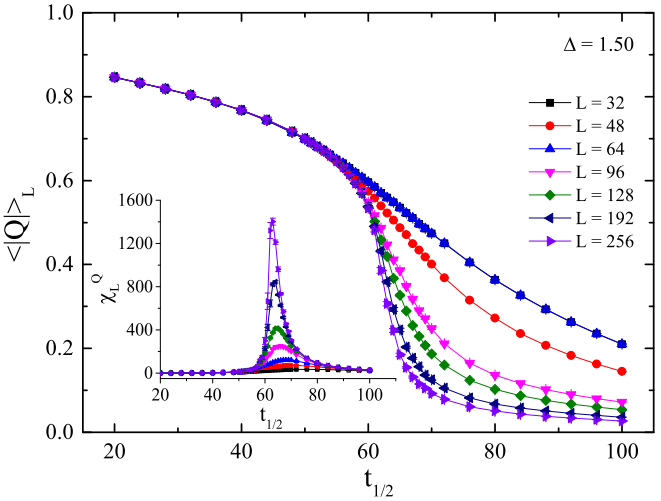

FIG. 5. Half-period dependency of the dynamic order parameter of the kinetic spin-1 $\Delta = 1.5$ Blume-Capel model for a wide range of system sizes studied. Inset: Half-period dependency of the corresponding dynamic susceptibility χ_L^Q.

To further explore the nature of the dynamic phase transition, we performed a finite-size scaling analysis of the simulation data obtained for various values of the crystal-field coupling Δ, as outlined above. Previous studies in the field indicated that although scaling laws and finite-size scaling are tools that have been designed for the study of equilibrium phase transitions, they also can be successfully applied to systems far from equilibrium, like the current kinetic spin-1 Blume-Capel model [27–31].

As an illustrative example of the case $\Delta = 1.5$, we present in Fig. 5 the finite-size behavior of the dynamic order parameter and in its inset the corresponding dynamic susceptibility for a wide range of system sizes studied. The figure clearly shows that this dynamic order parameter goes from a finite value to 0 values as the half-period increases, showing a sharp change around the value of the half-period that can be mapped to the corresponding peak in the plot of the dynamic susceptibility. The height and the location of the maximum χ_L^Q change with the system size and we may define these point locations as suitable pseudocritical half-periods, denoted hereafter $t_{1/2}^*$. The corresponding maxima may be similarly defined as $(\chi_L^Q)^*$. Moreover, the absence of finite-size effects below the critical point is a clear signature of a divergent length scale. Of course, similar plots may be prepared for all the other values of Δ studied, providing us with suitable pseudocritical points and susceptibility maxima that will allow us to perform finite-size scaling.

The shift behavior of the peak locations $t_{1/2}^*$ is plotted in Fig. 6 as a function of $1/L$ for all the values of the crystal-field coupling considered. Solid lines are fits of the usual shift form [63–65]

$$t_{1/2}^* = t_{1/2}^c + bL^{-1/\nu}, \tag{8}$$

where $t_{1/2}^c$ defines the critical half-period of the system and is a function of Δ and ν is the critical exponent of the correlation length. The obtained values for the critical half-period are listed in the third column in Table I. The relevant values for the

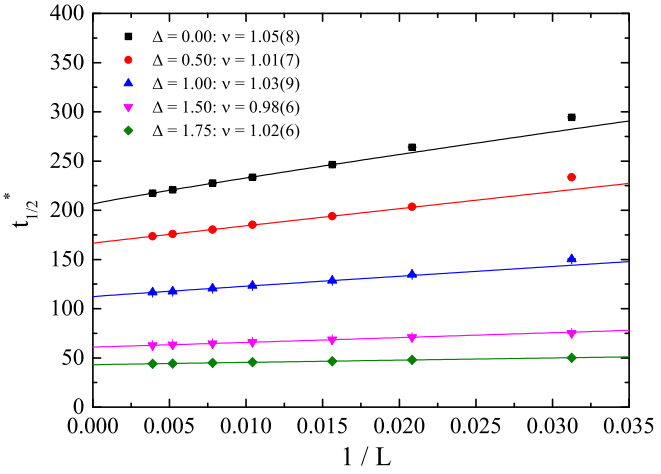

FIG. 6. Estimation of the critical half-period $t_{1/2}^c$ and the correlation length's exponent ν of the kinetic spin-1 Blume-Capel model for all values of Δ considered. Solid lines are fits of the form of (8).

critical exponent ν are given in the legend to Fig. 6 but are also listed in the fourth column in Table I. These values suggest that the critical exponent ν of the kinetic Blume-Capel model is compatible, up to a very good accuracy, with the value $\nu = 1$ of the 2D equilibrium Ising model, thus providing the first strong element of universality. Subsequently, in Fig. 7 we present the finite-size scaling analysis behavior of the peaks of the dynamic susceptibility and the solid lines are fits of the form [66]

$$(\chi_L^Q)^* \sim L^{\gamma/\nu}. \tag{9}$$

The results for the magnetic exponent ratio γ/ν are given in the legend to Fig. 7 and also in the fifth column in Table I. Again, these values for all Δ cases studied in the present work are in good agreement with the expected Ising value $\gamma/\nu = 1.75$, reinforcing the scenario of universality for the kinetic Blume-Capel model.

In addition to γ/ν, further evidence may be provided via the alternative magnetic exponent ratio, namely, β/ν, obtained

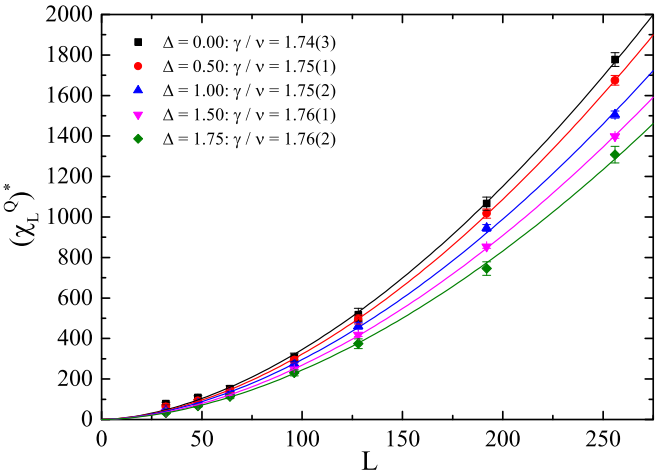

FIG. 7. Finite-size scaling analysis of the maxima $(\chi_L^Q)^*$ of the kinetic spin-1 Blume-Capel model for all values of Δ considered. Solid lines are fits of the form of (9).

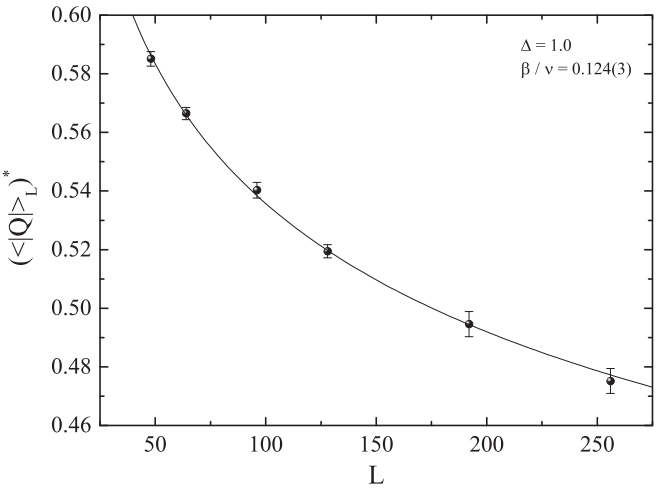

FIG. 8. Finite-size scaling analysis of the dynamic order parameter estimated at the critical half-period, $(\langle|Q|\rangle_L)^*$, of the 2D kinetic spin-1 Blume-Capel model at $\Delta = 1$. The solid line is a power-law fit of the form of (10).

from the scaling behavior of the dynamic order parameter at the critical point via

$$(\langle|Q|\rangle_L)^* \sim L^{-\beta/\nu}. \tag{10}$$

One characteristic example of this expected scaling behavior for the kinetic spin-1 Blume-Capel model is shown in Fig. 8 for $\Delta = 1$. A power-law fit of the form of (10) gives an estimate $0.124(3)$ for β/ν, in good agreement with the Ising value $1/8 = 0.125$. Let us note here that similar results have been obtained in our fitting attempts for all the other Δ values studied in this work.

As mentioned in Sec. III, we also measured the energy and its corresponding scaled variance, the heat capacity, (5). Both quantities are shown in Fig. 9 and its inset, respectively. Ideally, we would like to observe logarithmic scaling behavior of the maxima of the heat capacity $(\chi_L^E)^*$. Indeed, as shown in

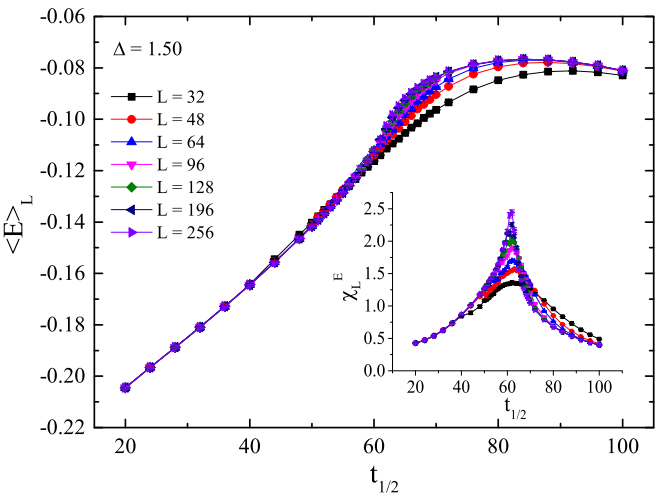

FIG. 9. Half-period dependency of the energy of the kinetic spin-1 $\Delta = 1.5$ Blume-Capel model for a wide range of system sizes studied. Inset: Half-period dependency of the corresponding heat capacity χ_L^E.

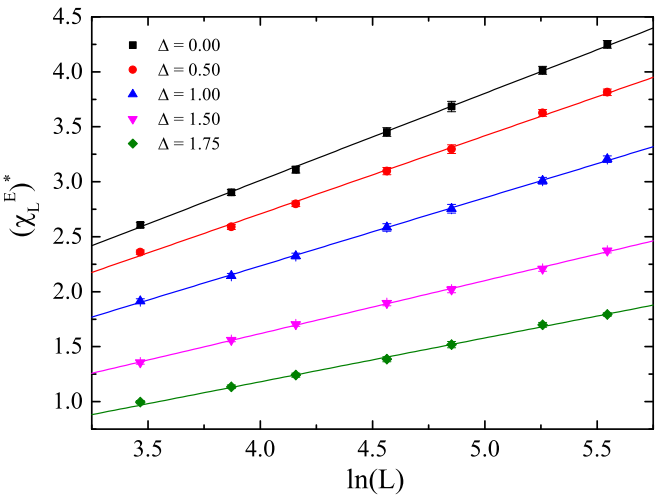

FIG. 10. Illustration of the logarithmic scaling behavior of the maxima of the heat capacity, $(\chi_L^E)^*$, for all values of Δ considered in this work. Solid lines are fits of the form of (11).

Fig. 10, the data for the maxima of the heat capacity show a clear logarithmic divergence of the form [67]

$$\left(\chi_L^E\right)^* \propto c_1 + c_2 \ln(L), \tag{11}$$

as expected for a 2D Ising ferromagnet.

A final verification of the equilibrium Ising universality class comes from the study of the Binder cumulant, as defined above for the case of the dynamic order parameter [see Eq. (7)]. In Fig. 11 we plot the fourth-order cumulant U_L for the case $\Delta = 1.5$ for the various system sizes considered in this work. The inset is a mere enlargement of the intersection area. The dashed vertical line marks the critical half-period value of the system $t_{1/2}^c = 61.0 \pm 0.3$, as estimated in Fig. 6, and the dotted horizontal line represents the universal value $U^* = 0.610\,692\,4(16)$ of the 2D equilibrium Ising model [68], which is consistent with the crossing point of our numerical

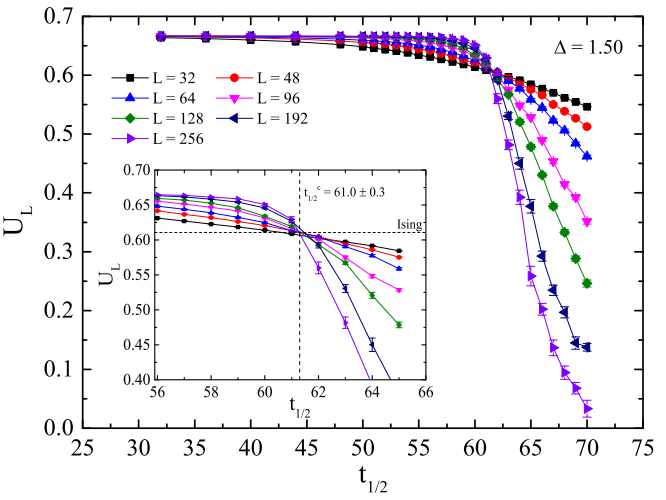

FIG. 11. Half-period dependency of the fourth-order Binder cumulant U_L of the kinetic spin-1 $\Delta = 1.5$ Blume-Capel model for a wide range of system sizes studied. Inset: An enhancement of the intersection area.

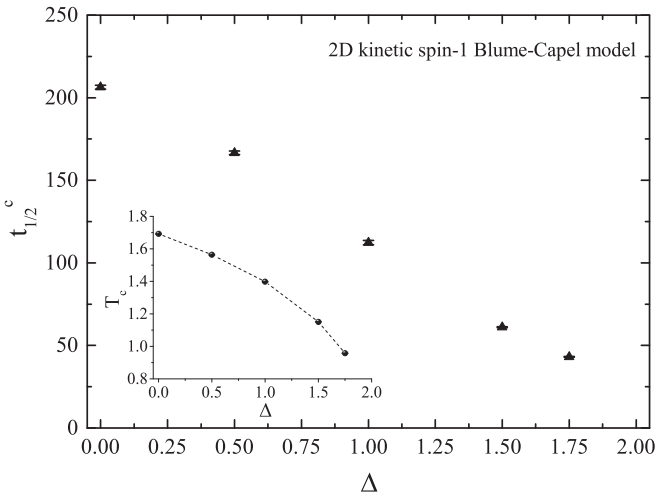

FIG. 12. Dynamic $\Delta - t_{1/2}^c$ phase boundary of the kinetic spin-1 square-lattice Blume-Capel model. Inset: For the sake of completeness we provide a part of the phase diagram of the equilibrium counterpart on the $(\Delta - T_c)$ plane using the results from Ref. [47] that were used in the present work. The dotted line is a simple guide for the eye.

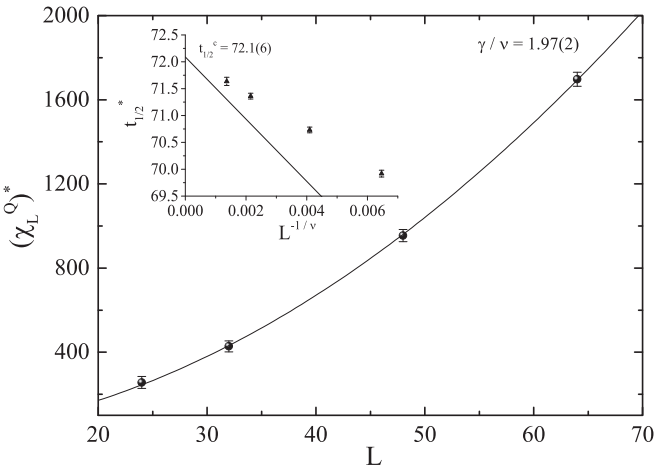

FIG. 13. Finite-size scaling analysis of the maxima $(\chi_L^Q)^*$. Inset: Shift behavior of the corresponding pseudocritical half-periods $t_{1/2}^*$ of the 3D kinetic spin-1 Blume-Capel model.

data. Certainly, the crossing point is expected to depend on the lattice size L (as also shown in the figure) and the term universal is valid for given lattice shapes, boundary conditions, and isotropic interactions. For a detailed discussion of this topic we refer the reader to Refs. [69] and [70]. Still, the scope of the current Fig. 11 is to show qualitatively another instance of the Ising universality. Similar plots and conclusions hold also for the other values of Δ studied but are omitted for brevity. As a note, we remind the reader that an alternative way to estimate the critical exponent ν comes from the scaling behavior of the derivative of the Binder cumulant at the corresponding crossing points, via $(\partial U_L/\partial t_{1/2}) \propto L^{1/\nu}$, an approach that demands quite accurate data at the area of the crossing points for safe estimation of derivatives [58].

We complete our analysis of the 2D model by presenting in Fig. 12 an illustrative formulation of a dynamic phase diagram for the kinetic spin-1 Blume-Capel model on the $(\Delta - t_{1/2}^c)$ plane, using the values for the critical half-period listed in Table I. We also include a complementary inset with the corresponding equilibrium counterpart on the $(\Delta - T_c)$ plane using the results in Ref. [47] for the regime of continuous transitions. As shown in Fig. 12, the values of $t_{1/2}^c$ decrease almost linearly with increasing Δ. We are not currently sure whether this is due to the particular selection of the chosen temperatures, $0.8T_c(\Delta)$, or is a general result for any temperature well below T_c. Further simulations are needed to clarify this point, but they are beyond the scope of the current study.

V. ON THE DYNAMIC PHASE TRANSITION OF THE 3D BLUME-CAPEL MODEL

In this section we present some complementary results on the dynamic phase transition of the kinetic spin-1 3D Blume-Capel model, as defined in Eq. (1), but with the spins living on the simple cubic lattice. In this case $N = L \times L \times L$, where $L \in \{8,16,24,32,48,64\}$. The analysis below is presented for a single value of the crystal-field coupling in the second-order transition regime of the phase diagram, namely, for $\Delta = 0.655$. For this value of Δ, the critical temperature of the model has been very accurately determined by Hasenbusch to be $T_c = 2.579\,169$ [71]. Our Monte Carlo simulations followed the protocol defined in Sec. II for the case of the square-lattice model, using now $h_0 = 0.6$ and $T = 0.8T_c$ as appropriate choices for the magnetic-field strength and the temperature, respectively.

We summarize our results in Figs. 13–15. In particular, in Fig. 13 we present the finite-size scaling behavior of the maxima $(\chi_L^Q)^*$. The solid line is a fit of the form of (9), providing us with the estimate $\gamma/\nu = 1.97(2)$, which is in very good agreement with the Ising value 1.963 70(2) of the equilibrium 3D Ising ferromagnet [72]. In the corresponding inset we illustrate the shift behavior of the pseudocritical half-periods $t_{1/2}^*$ as a function of $L^{-1/\nu}$, where ν has been

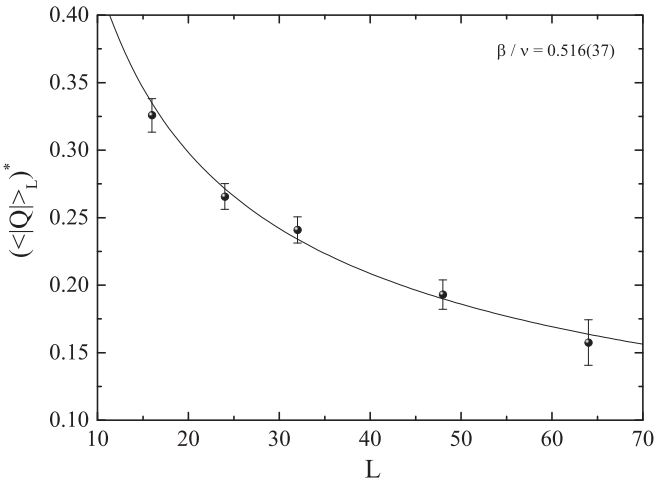

FIG. 14. Finite-size scaling analysis of the dynamic order parameter estimated at the critical half-period, $(\langle |Q| \rangle_L)^*$, of the 3D kinetic spin-1 Blume-Capel model. The solid line is a power-law fit of the form of (10).

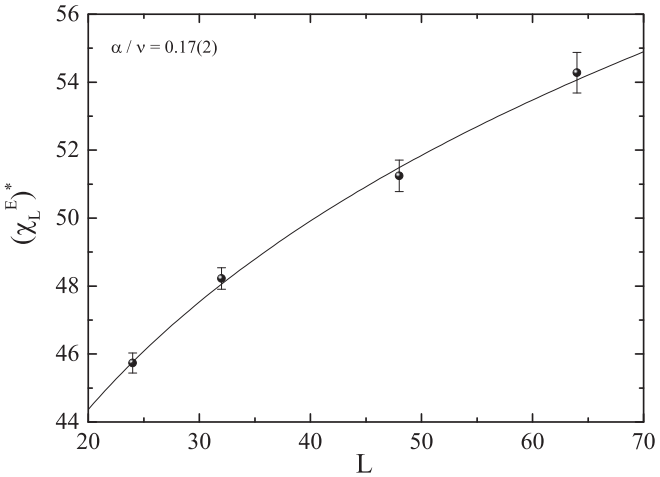

FIG. 15. Finite-size scaling analysis of the maxima $(\chi_L^E)^*$ of the 3D kinetic spin-1 Blume-Capel model. The solid line is a power-law fit of the form of (12).

fixed at the Ising value 0.629 971 [72]. The numerical data are well described by a linear extrapolation to the $L \to \infty$ limit [see also Eq. (8)], indicating that the critical exponent ν of the kinetic version of the 3D Blume-Capel model shares the value of its equilibrium counterpart. The critical half-period is also estimated to be $t_{1/2}^c = 72.1 \pm 0.6$ for the particular case of Δ studied here, as also indicated in the inset in Fig. 13.

Figure 14 illustrates the scaling behavior of the dynamic order parameter of the 3D kinetic spin-1 Blume-Capel model at the above estimated critical half-period, $(\langle |Q| \rangle_L)^*$. Similarly to the 2D model, the solid line is a power-law fit of the form of (10), providing the estimate $\beta/\nu = 0.516(37)$ for the magnetic exponent ratio, to be compared with the value 0.5181 49(6) of the 3D Ising model [72]. Again, the agreement is beyond any (numerical) doubt.

Finally, we discuss the scaling behavior of the heat capacity, (5). In Fig. 15 we present the size evolution of the maxima of the heat capacity $(\chi_L^E)^*$ of the 3D kinetic spin-1 Blume-Capel model. The solid line is a power-law fit of the form [64]

$$\left(\chi_L^E\right)^* \sim L^{\alpha/\nu}, \tag{12}$$

and the obtained estimate for the critical exponent ratio $\alpha/\nu = 0.17(2)$ nicely compares to the equilibrium value $\alpha/\nu = 0.17475(2)$ of the 3D Ising ferromagnet [72], thus supporting the conclusion of the earlier work by Park and Pleimling on the 3D kinetic Ising model [31].

VI. SUMMARY

In the present work we have investigated the dynamical response of the 2D Blume-Capel model exposed to a square-wave oscillating external field. Using Monte Carlo simulations and finite-size scaling techniques we have studied the system at various values of the crystal-field coupling within the second-order transition regime. Our results for the critical exponent ν, the magnetic exponent ratios γ/ν and β/ν, the universal Binder cumulant, and the observed logarithmic divergence of the heat capacity indicate that the present nonequilibrium phase transition belongs to the universality class of the equilibrium Ising model. Furthermore, with the numerical data at hand, we have been able to construct a 2D dynamic phase diagram for the range of parameters considered, in analogy with the equilibrium case. Additional evidence in favor of this universality scenario between the dynamic phase transition and its equilibrium counterpart has been provided via a supplemental study of the 3D Blume-Capel model.

To conclude, the results presented in the current paper, together with existing results for the 2D and 3D kinetic Ising models [27–33], establish a clear universality between the equilibrium and the dynamic phase transitions of Ising spin models. They also provide additional support for the symmetry arguments put forward by Grinstein *et al.* [73] a few decades ago, underlying the role of symmetries in nonequilibrium critical phenomena.

ACKNOWLEDGMENTS

The authors would like to thank P. A. Rikvold and W. Selke for many useful comments on the manuscript. The numerical calculations reported in this paper were performed at Tübitak Ulakbim (Turkish agency), High Performance and Grid Computing Center (TRUBA Resources).

[1] T. Tomé and M. J. de Oliveira, Phys. Rev. A **41**, 4251 (1990).
[2] W. S. Lo and R. A. Pelcovits, Phys. Rev. A **42**, 7471 (1990).
[3] M. F. Zimmer, Phys. Rev. E **47**, 3950 (1993).
[4] M. Acharyya and B. K. Chakrabarti, Phys. Rev. B **52**, 6550 (1995).
[5] B. K. Chakrabarti and M. Acharyya, Rev. Mod. Phys. **71**, 847 (1999).
[6] M. Acharyya, Phys. Rev. E **56**, 1234 (1997).
[7] M. Acharyya, Phys. Rev. E **69**, 027105 (2004).
[8] G. M. Buendía and E. Machado, Phys. Rev. E **58**, 1260 (1998).
[9] G. M. Buendía and E. Machado, Phys. Rev. B **61**, 14686 (2000).
[10] H. Jang, M. J. Grimson, and C. K. Hall, Phys. Rev. E **68**, 046115 (2003).
[11] H. Jang, M. J. Grimson, and C. K. Hall, Phys. Rev. B **67**, 094411 (2003).
[12] X. Shi, G. Wei, and L. Li, Phys. Lett. A **372**, 5922 (2008).
[13] A. Punya, R. Yimnirun, P. Laoratanakul, and Y. Laosiritaworn, Physica B **405**, 3482 (2010).
[14] P. Riego and A. Berger, Phys. Rev. E **91**, 062141 (2015).
[15] M. Keskin, O. Canko, and U. Temizer, Phys. Rev. E **72**, 036125 (2005).
[16] M. Keskin, O. Canko, and Ü. Temizer, J. Exp. Theor. Phys. **104**, 936 (2007).
[17] D. T. Robb, P. A. Rikvold, A. Berger, and M. A. Novotny, Phys. Rev. E **76**, 021124 (2007).
[18] B. Deviren and M. Keskin, J. Magn. Magn. Mater. **324**, 1051 (2012).
[19] Y. Yüksel, E. Vatansever, and H. Polat, J. Phys.: Condens. Matter **24**, 436004 (2012).

[20] Y. Yüksel, E. Vatansever, U. Akinci, and H. Polat, Phys. Rev. E **85**, 051123 (2012).
[21] E. Vatansever, Phys. Lett. A **381**, 1535 (2017).
[22] Y.-L. He and G.-C. Wang, Phys. Rev. Lett. **70**, 2336 (1993).
[23] D. T. Robb, Y. H. Xu, O. Hellwig, J. McCord, A. Berger, M. A. Novotny, and P. A. Rikvold, Phys. Rev. B **78**, 134422 (2008).
[24] J.-S. Suen and J. L. Erskine, Phys. Rev. Lett. **78**, 3567 (1997).
[25] A. Berger, O. Idigoras, and P. Vavassori, Phys. Rev. Lett. **111**, 190602 (2013).
[26] P. Riego, P. Vavassori, and A. Berger, Phys. Rev. Lett. **118**, 117202 (2017).
[27] S. W. Sides, P. A. Rikvold, and M. A. Novotny, Phys. Rev. Lett. **81**, 834 (1998).
[28] S. W. Sides, P. A. Rikvold, and M. A. Novotny, Phys. Rev. E **59**, 2710 (1999).
[29] G. Korniss, C. J. White, P. A. Rikvold, and M. A. Novotny, Phys. Rev. E **63**, 016120 (2000).
[30] G. M. Buendía and P. A. Rikvold, Phys. Rev. E **78**, 051108 (2008).
[31] H. Park and M. Pleimling, Phys. Rev. E **87**, 032145 (2013).
[32] K. Tauscher and M. Pleimling, Phys. Rev. E **89**, 022121 (2014).
[33] E. Vatansever, arXiv:1706.03351.
[34] H. Park and M. Pleimling, Phys. Rev. Lett. **109**, 175703 (2012).
[35] G. M. Buendía and P. A. Rikvold, Phys. Rev. B **96**, 134306 (2017).
[36] H. W. Capel, Physica (Amsterdam) **32**, 966 (1966).
[37] M. Blume, Phys. Rev. **141**, 517 (1966).
[38] I. D. Lawrie and S. Sarbach, in *Phase Transitions and Critical Phenomena*, Vol. 9, edited by C. Domb and J. L. Lebowitz (Academic Press, London, 1984).
[39] W. Selke and J. Oitmaa, J. Phys.: Condens. Matter **22**, 076004 (2010).
[40] A. N. Berker and M. Wortis, Phys. Rev. B **14**, 4946 (1976).
[41] N. S. Branco and B. M. Boechat, Phys. Rev. B **56**, 11673 (1997).
[42] D. P. Snowman, Phys. Rev. E **79**, 041126 (2009).
[43] A. K. Jain and D. P. Landau, Phys. Rev. B **22**, 445 (1980).
[44] A. Falicov and A. N. Berker, Phys. Rev. Lett. **74**, 426 (1995).
[45] C. J. Silva, A. A. Caparica, and J. A. Plascak, Phys. Rev. E **73**, 036702 (2006).
[46] A. Malakis, A. N. Berker, I. A. Hadjiagapiou, and N. G. Fytas, Phys. Rev. E **79**, 011125 (2009).
[47] A. Malakis, A. N. Berker, I. A. Hadjiagapiou, N. G. Fytas, and T. Papakonstantinou, Phys. Rev. E **81**, 041113 (2010).
[48] A. Malakis, A. N. Berker, N. G. Fytas, and T. Papakonstantinou, Phys. Rev. E **85**, 061106 (2012).
[49] N. G. Fytas and W. Selke, Eur. Phys. J. B **86**, 365 (2013).
[50] W. Kwak, J. Jeong, J. Lee, and D.-H. Kim, Phys. Rev. E **92**, 022134 (2015).
[51] J. Zierenberg, N. G. Fytas, M. Weigel, W. Janke, and A. Malakis, Eur. Phys. J. Special Topics **226**, 789 (2017).
[52] N. Boccara, A. Elkenz, and M. Saber, J. Phys.: Condens. Matter **1**, 5721 (1989).
[53] W. Hoston and A. N. Berker, Phys. Rev. Lett. **67**, 1027 (1991).
[54] H. Ez-Zahraouy and A. Kassou-Ou-Ali, Phys. Rev. B **69**, 064415 (2004).
[55] X. Shi and G. Wei, Phys. Scripta **89**, 075805 (2014).
[56] M. Acharyya and A. Halder, J. Magn. Magn. Mater. **426**, 53 (2017).
[57] N. Metropolis, A. W. Rosenbluth, M. N. Rosenbluth, A. H. Teller, and E. Teller, J. Chem. Phys. **21**, 1087 (1953).
[58] D. P. Landau and K. Binder, *A Guide to Monte Carlo Simulations in Statistical Physics* (Cambridge University Press, Cambridge, UK, 2000).
[59] M. E. J. Newman and G. T. Barkema, *Monte Carlo Methods in Statistical Physics* (Oxford University Press, New York, 1999).
[60] R. J. Glauber, J. Math. Phys. **4**, 294 (1963).
[61] W. H. Press, S. A. Teukolsky, W. T. Vetterling, and B. P. Flannery, *Numerical Recipes in C*, 2nd ed. (Cambridge University Press, Cambridge, UK, 1992).
[62] K. Binder, Z. Phys. B: Condens. Matter **43**, 119 (1981); Phys. Rev. Lett. **47**, 693 (1981).
[63] M. E. Fisher, *Critical Phenomena*, edited by M. S. Green (Academic Press, London, 1971).
[64] V. Privman, *Finite Size Scaling and Numerical Simulation of Statistical Systems* (World Scientific, Singapore, 1990).
[65] K. Binder, *Computational Methods in Field Theory*, edited by C. B. Lang and H. Gausterer (Springer, Berlin, 1992).
[66] A. M. Ferrenberg and D. P. Landau, Phys. Rev. B **44**, 5081 (1991).
[67] A. E. Ferdinand and M. E. Fisher, Phys. Rev. **185**, 832 (1969).
[68] J. Salas and A. D. Sokal, J. Stat. Phys. **98**, 551 (2000).
[69] W. Selke, J. Stat. Mech. (2007) P04008.
[70] W. Selke and L. N. Shchur, Phys. Rev. E **80**, 042104 (2009).
[71] M. Hasenbusch, Phys. Rev. B **82**, 174434 (2010).
[72] F. Kos, D. Poland, D. Simmons-Duffin, and A. Vichi, J. High Energy Phys. 08 (2016) 036.
[73] G. Grinstein, C. Jayaprakash, and Y. He, Phys. Rev. Lett. **55**, 2527 (1985).